Comparative study of polymorphous Alzheimer's Aβ(1-40) amyloid nanofibrils and microfibers

Raffaella Paparcone*, Joseandres Sanchez* and Markus J. Buehler*,†

** Laboratory for Atomistic and Molecular Mechanics, Department of Civil and Environmental Engineering, Massachusetts Institute of Technology, 77 Massachusetts Ave. Room 1-235A&B, Cambridge, MA, USA*

† *Corresponding author, electronic address: mbuehler@MIT.EDU, Phone: +1-617-452-2750, Fax: +1-617-324-4014*

ABSTRACT: The class of amyloid protein materials are associated with severe degenerative diseases, such as Parkinson's disease, Alzheimer's disease and type II diabetes. Moreover, they represent an intriguing class of protein molecules that show exceptional strength, sturdiness and elasticity. However, physical models that explain the structural basis of these properties remain largely elusive. This is partly due to the fact that structural models of microscale amyloid fibrils remain unknown, preventing us from pursuing bottom-up studies to describe the link between their hierarchical structure and physical properties. Here we focus on the β-amyloid peptide Aβ(1-40), which is associated with Alzheimer's disease. Earlier experimental studies suggest that this amyloid fibril arranges in both double and triple layered β-sheet structures, leading to twofold and threefold morphologies. The resulting structures are stabilized by a hydrophobic core and interprotein H-bond networks. Here we identify the atomistic coordinates of both twofold and threefold morphologies, providing a structural fiber model with lengths of hundreds of nanometers. We present a systematic comparison between the two morphologies, including energetic properties, structural changes and H-bonding patterns, for varying fibril lengths. Our results suggest that the double layered morphology is more stable than the threefold morphology. The model described here predicts the formation of twisted amyloid microfibers with a periodicity of ≈133 nm and ≈82 nm, for the twofold and threefold structures, respectively. The approach proposed here makes a direct connection from the atomistic to the mesoscale level, provides a link between the fibril

geometry, the chemical interactions and the final more stable configuration, and resolves the issue of missing atomistic structures for long amyloid fibers.

Keywords: Amyloid structure, molecular dynamics, fibrillar proteins, structure prediction, computational materiomics, polymorphism

Accepted for publication in: *Journal of Computational and Theoretical Nanoscience*

1. Introduction

Amyloids are highly organized, hierarchical fibrillar protein aggregates that form from a large class of peptides and proteins with disparate sequences (Figure 1). Amyloids are associated with severe degenerative disorders including Alzheimer's disease, Parkinson's disease, type II diabetes and transmissible spongiform encephalopaties [1]. The conversion of biologically functional proteins from the native soluble state to the amyloid configuration causes the catastrophic loss of their solubility, and most importantly, their functionality. Earlier experimental studies have indeed confirmed the toxicity of amyloid precursors [2]. However, the specific role of amyloids in the above mentioned medical disorders is not well understood, resulting in a need to identify their structure and properties to clarify formation mechanisms and structure-property links. In addition to their role in diseases, amyloids have also been discussed as an example of a highly ordered, hierarchical material with exceptional mechanical and structural properties. For example, earlier studies identified that amyloids also play an important role in natural adhesives [3], suggesting that amyloids are also associated with normal physiological mechanisms in biology. Amyloids appear to be a stable structural state of generic polypeptide chains, and as such could be used as a template for the development of new self-organized nanomaterials (e.g. nanowires) [4-6]. However, it remains an open question how atomistic details of small structures (e.g. the amino acid sequence) at nanoscale translate to properties at much larger scales, currently preventing us from fully exploiting amyloids as a new generation nanomaterial. Computational nanoscience, and a systematic materiomics approach to identify the role of amyloids in

biomedical disorders, is a promising approach that could help us in elucidating the functional material properties of amyloids.

Amyloids feature filamentous aggregates (so-called plaques), with typical fiber diameters of ≈10 nm and fiber lengths of the order of micrometers (see Figure 1A). The fact that amyloids are inherently insoluble and non-crystalline prevented the determination of their molecular structure using common experimental approaches (such as nuclear magnetic resonance, NMR, and x-ray crystallography). Only recent progress in the application of solid-state NMR (ssNMR) [7-9] and in growing peptide elongated microcrystals has provided detailed structural and biochemical information on amyloids [10]. In particular, these studies revealed that the molecules composing the fibrils posses a degree of order that has previously only been associated with crystalline materials (such as metals or ceramics), and not with proteins. In fact, x-ray diffraction patterns of aligned amyloid fibrils allowed to define the structural core as a set of β-sheets oriented in parallel to the fibril axis, with their strands perpendicular to this axis [10]. Since this regularity can be detected through the resonance lines of ssNMR, it is expected that complete atomistic-level structures will be available for many other amyloidic systems (whose detailed description is currently still missing). Despite progress in structure identification, many of the fundamental properties, specifically their strength, sturdiness and great elasticity, are not fully understood. This is partly due to the fact that larger-scale structural models of amyloid fibrils remain elusive, preventing bottom-up theoretical and computational studies to describe their nanomechanical properties. Most known structural models of amyloid fibrils are limited to lengths of several nanometers (or a few layers of protein). However, relevant functional and biologically active properties (and properties for potential nanotechnology applications) emerge at scales of hundreds of nanometers and micrometers (see, e.g. Figure 1B where the interaction of amyloid plaques with neuron cells is schematically shown).

In the last few years, significant progress has been made in theoretical and computational studies providing the first models of the peptide-level structure of amyloids, as well as for the formation mechanisms of the amyloid fibrils [11].These studies have been focused on a range

of different systems that include primarily smaller sequences, such as polyalanine peptides [12], Aβ-peptides [13, 14], calcitonine [15] and β_2 –microglobuline [16-18]. Some studies focused on larger structures like prion proteins [19]. In 2002, a computational study [20] and an experimental investigation [7] independently proposed a rather similar model for the Aβ (1-42) peptide amyloid. Theory and experiment agreed rather well, and both found that the most basic peptide building block is a U-turn bent β-sheet (also referred to as "β-unit").

This Aβ (1-42) peptide is directly related to the Alzheimer's disease. It is formed after sequential cleavage of the Amyloid Precursor Protein (APP) that is expressed in many tissues and concentrated in the synapses of neurons. The successive actions of the α- γ-secretases generates the Aβ proteins that can be present in many different isoforms. Among them, the most common are the Aβ(1-40) and Aβ(1-42) structures. These peptides, and in particular their associated amyloidic fibrils, are being extensively studied especially by ssNMR, and a wide range of information on their atomistic structures and configurations are now available [7, 21]. The basic structure is a single β-unit stabilized by a salt bridge and the overall fiber consists of the repetition of units of these along the fiber axis. The so-formed layers stack in register, and the stability of the resulting fibrous structure depends on a dense and highly organized network of hydrogen bonds (H-bonds). In a recent article, the presence of two distinct morphologies for the Aβ(1-40) protein has been suggested [9], a twofold and threefold morphology (see Figure 2). Specifically, Tycko and coworkers observed two types of amyloid fibers that are periodically twisted around the growth axis, confirming the existence of polymorphism in amyloid fibrils [9]. Both morphologies contain in register parallel β-sheets, but differ in the overall symmetry (that is, twofold versus threefold), the conformation of non β-strand traits, as well as certain quaternary contacts [9]. According to experimental imaging, the twofold fibril morphology is characterized by a striated ribbon, while most of the threefold fibrils display a periodically twisted morphology. In the last case, a molecular-level model of short segments of amyloid fibrils composed of 6 layers (of ≈30 Å length) has recently been described in the literature based on solid state NMR data [7, 9]. However, this study did not result in larger-scale structural models of amyloid fibrils.

Specifically, the twist angle, periodicity and atomic structure at scales of hundreds of nanometers remains elusive, preventing a direct comparison with TEM based imaging of amyloid fibrils. A large scale structure is thus needed for further studies to contribute to the general understanding of amyloids properties.

In a recent paper we proposed a model to predict the atomistic coordinates of the threefold morphology fibers at the scale of hundred of nanometers, on the basis of structural and energetic considerations [22]. Here, we apply the same method to the twofold morphology and provide a description of the geometrical and energetic changes that can be observed when fibers feature an increasing length and different symmetries. In qualitative agreement with experimental evidence, we find a twisted periodicity for both the twofold and threefold symmetry structures. We also find a twist periodicity for the twofold morphology, a phenomenon that has not yet been observed experimentally. We then report a systematic between the two morphologies with increasing fibril length, and propose a model for the prediction of micrometer scale structures of these amyloid fibrils. Our study represents a multi-scale approach that could find further applications in both experimental and theoretical studies.

2. Methods

2.1 Fiber geometry setup

The amino acid sequence of the studied Aβ(1–40) amyloid fibrils is DAEFRHDSGYEVHHQKLVFFAEDVGSNKGAIIGLMVGGVV. In this paper, small structures (with lengths in the range of Ångstroms to a few nanometers) are referred to as fibrils, while much longer structures (with lengths in the range of tens of nanometers and longer) are referred to as fibers. In both the twofold and threefold morphology, we build increasingly long fibrils by adopting a systematic strategy. It consists of selecting one layer in the original structure, copying and translating it along the fibril axis N times (where N=2, 3...20, 25, 30, 40), imposing a typical inter-strand distance of the β-sheet configuration as the

starting distance (d = 4.8 Å). In both cases the longest simulated fibril is ≈190 Å long. No rotation is imposed between the layer copies in the initial configuration.

2.2 Atomistic simulation approach

The built structures are minimized to relax strain, and then equilibrated using the implicit solvent model implemented in the CHARMM force field model (EEF1) [23], implemented in the CHARMM simulation code [24]. The minimization consists of 10,000 Steepest Descent (DS) steps followed by 50,000 Adopted Basis Newton-Raphson Method steps. The subsequent relaxation is performed using the Velocity-Verlet algorithm (VV2) for 1000 ps (time step=0.001 ps), at a constant temperature of 300 K. No other constraints are imposed to the system.

2.3 Geometrical parameter identification

Figure 2 schematically depicts the method we used to get the overall top-bottom (D) distance and twist angle (Θ) of the relaxed structures. In both morphologies we considere the positions of the serine residues as reference points (two and three, respectively, for the two morphologies) in the top and bottom layers. This choice is justified by the fact that the positions of this residue are almost in the center of each chain, and therefore are least affected by entropic fluctuations acting on the tails of each chain composing the layers. For the two- and threefold morphologies, the final values of D and Θ are calculated as the average of two and three values, respectively. The obtained geometrical parameters are then normalized by the number of layers (N) that constitute the structure, thereby providing the corresponding values of the interstrand twist angle (θ) and distance (d).

3. Results and discussion

Our analysis starts from a single peptide layer as shown in Figure 2, for both morphologies. Fibrils of increasing lengths are built following the approach described in section 2. After minimization and relaxation, we observe that the geometry of all the protein fibrils converges, and each structure displays a twist angle between adjacent layers with respect to

the growth axis. Specifically, in the twofold morphology, the structure shows almost the same variation of the twist angle during the minimization and equilibration processes. For instance, in the case of fibril composed of 20 layers, the measured variation of the interlayer angle is 0.84° and 0.45° after the minimization and equilibration, respectively. In the threefold morphology, instead, the structure twists only slightly during the energy minimization, while it shows significant twist angle formation during the finite temperature equilibration process. In the 20 layers fibril, for example, the variation of the twist angle during the energy minimization and during the subsequent equilibration corresponds to 0.82° and 1.66°, respectively. This observation suggests that twist formation is driven not only by entropic effects, but also by the geometric properties of the fibrils. This confirms a hypothesis that has been discussed in the literature [25].

The occurrence of a twist angle has been observed as a common feature of many β-sheets structures. Several earlier studies have been reported, and different explanations have been proposed. They address many diverse aspects, including the entropy associated with the backbone degrees of freedom [25, 26], the out-of-plane deformation of peptide groups [27], intrastrand [28-30] and tertiary interactions [31, 32]. Moreover, in 2005 Koh and Tim proposed that the degree of twist should be determined by the tendency to minimize the surface area of the system [33]. This conclusion seems to qualitatively agree with our findings. In the twofold case, the twist movement has as direct consequence the increase of the contact surface of the highly hydrophobic internal core of the fibril. In this case the hydrophobic interactions represent the main driving force for achievement of structural stability, while the occurring twisting movement during both the minimization and the equilibration gives only a limited contribution. In the threefold morphology, instead, the twist movement offers the structure the best path to reach the minimum energy conformation. The intrinsic geometry of the fibril includes long and highly stiff sets of β-sheets that prevent the hydrophobic inner sides to come closer. Thereby, they only allow a twist movement that is wider than the one observed in the twofold morphology. Moreover, the threefold morphology shows a larger variation of the twist angle during the equilibration. In this case, the final

configuration appears to be the result of the combination of entropic [25], structural and geometric effects.

Figure 3 displays a sample structure morphology with $N = 9$ layers after the relaxation procedure. They clearly present a twist angle along the fibril axis in both the two- and three-fold fibrils. The occurrence of the axial twist qualitatively agrees with the published threefold structure of the Aβ(1-40) peptide [9] and suggests that the same concept also holds for the two-fold morphology. Thus far, it has been described only as "striated ribbon" morphology [9] and the occurrence of a twisted structure has not yet been directly observed.

3.1 Energetic analysis

In order to identify the energetic and structural changes during fiber growth, we calculate the potential energy per layer, as a function of the number of layers in the amyloid fibril. This contributes to elucidate the crucial driving forces in the assembly process of amyloids. Figure 4A and B report the fibril energy as function of the length in both the two and threefold morphologies. It is evident that, for both the morphologies, short fibrils feature a strong dependence of the average energy associated to the addition of a new layer. However, a plateau is reached for fibrils with more than 20-30 layers, suggesting that adding a new layer to an existing fibril remains an energetically favorable process that does not depend on the length of the growing fibril. This observation suggests that the stronger energetic driving force for ultra-small fibrils may explain the strong propensity towards further growth once an amyloid critic fibril length is reached. From the energy values extrapolated from the plots reported in Figure 4, we evaluate the difference in potential energy per turn and per layer between the twofold and the threefold morphologies. This difference, estimated to be ΔE = 22.011 kcal/mol, suggests that the twofold morphology is more stable. This can be explained by addressing the distinct geometric and chemical features of the two morphologies, as discussed in the next section.

3.2 Structure analysis

Here we present further investigations to identify the geometric properties of the fibrils. Specifically we determine the twist angle θ and the interlayer distance d for the final relaxed structures according to the method described above.

In Figure 5A and B we report the geometrical parameters, d and θ as function of the number of layers composing the fiber for the two- and threefold morphology, respectively. Interestingly, similar as in the case of the energy, we find that, in both cases, 20-30 layers corresponds to a critical fiber length at which the geometric parameters become length-independent. The extrapolated asymptotic values for the interstrand distance and twist angle are reported in Table 1. This result represents a geometrical confirmation that the extrapolated parameters could actually be used to define the structure of longer fibers opening the possibility to shed light on systems that reaches the length of hundreds of nanometers and micrometers.

The change of the number of H-bonds from the starting structure to the minimized and then to the relaxed one, enables us to carry out an evaluation of the variation in the chemical interactions stabilizing the fibril. In Figure 6 the profile of such a number, for the starting, minimized and relaxed structure, is reported as function of the fibril length for the twofold and threefold morphologies (Figures 6A and B, respectively). The analysis shows that the energy minimization step has a distinct effect on the number of H-bonds between the twofold and the threefold morphologies. In the first case, the number of H-bonds decreases from the starting configuration with the subsequent processes of minimization and relaxation. In the second case there is a clear increase of the H-bonds interaction, suggesting that the different symmetry of the two morphologies could play a very important role.

Overall, there are two distinct contributions to the improvement of structural stability: the hydrophobic interactions, and H-bonding. In the twofold structure, the geometry of the fibril allows the highly hydrophobic inner part of each U-turn to come close, promoting the twist movement and the increase of the contact surface of the hydrophobic core constituting the fibril. The decrease of the number of H-bonds is then replaced and compensated by the new

and increased contact area promoted by the hydrophobic interactions. In the threefold morphology, instead, the three stiff networks of β-sheets parallel to the fibril axis prevent the hydrophobic internal segments to come close and therefore, the only path the molecule can follow to minimize its energy is represented by the twist movement and by the increase of the number of the H-bonds. This explanation is supported by the larger twist angle observed in the threefold morphology (as discussed above and shown in Table 1), and by the different relaxed configurations found for twofold fibrils with few layers (less than 4 layers as shown in Figure 7).The analysis of the relaxed configurations of very short fibrils (2, 3 and 4 layers) reveals the occurrence of diverse types of interactions, and shows that for extremely short fibrils there is a competition between the hydrophobic interactions and the formation of H-bonds.

In Figure 7, the relaxed twofold (subplot A) and threefold (subplot B) morphology structures consisting of 2, 3 and 4 layers are depicted. The inner part of each chain is distinguished by the blue color. In the twofold morphology, the shortest structure consisting of only 2 layers loses its small contact area and this loss is compensated by the formation of strong antiparallel β-sheets showing that in this case, H-bond formation drives the configuration toward the most stable geometry (Figure 7A) In structures that feature the twofold symmetry and consist of 3 layers, the relaxed configuration shows how the increased hydrophobic interactions and the wider contact area start playing a more important role in driving the structure towards its final configuration. This occurs when the structure reaches a length of 4 layers. The opposite process can be observed in the threefold morphology (Figure 7B). For systems consisting of 2 or 3 layers, even though the geometry imposes a big distance between the hydrophobic inner parts, the β-sheet sets composing each side are too short to prevent the inner hydrophobic segments to come close. As the number of layers increases the stiffness of the longer β-cross networks becomes higher: the threefold geometry is kept, and the hydrophobic interactions cannot drive the structure towards its final configuration.

3.3 Evaluation of the periodicity

The results reported in the previous section show that the properties of a fibril that is at least ≈20 layers long (≈96 Å) can be used to predict the structure of fibers of any length in both the cases of twofold and threefold symmetry. Moreover, using the parameters d and θ it is possible to evaluate the total periodicity of the predicted fibers ν, where ν is defined as the minimum length of a fiber to run over a complete turn, that means the length to cover a twist angle of 360°. Using the extrapolated interstrand twist angle and distance reported in Table 1, we calculate the periodicity as $\nu = 360 \times d/\theta$. The values we obtain for the twofold and the threefold morphology are ≈131.6 nm and ≈82.3 nm respectively. The experimental periodicity has been defined as the distance between apparent minima in the fibril width, as can be observed in negatively stained transmission electron microscope images [9].

The experimentally measured periodicity for the threefold morphology is 120±20 nm [9] (the definition given for a threefold symmetry implies that the fiber length needed to cover a complete turn is three times this value, corresponding to our definition of periodicity). The difference between the experimental and predicted values of the fiber periodicity could perhaps be explained by taking into account the fact that the predicted fiber geometry is an extrapolation based on a perfect structure, which does not include any geometric defects in the overall structure. In experimentally measured fibers the presence of local defects may reduce the effective twist angle, which results in larger periodicity values. Indeed, we have observed in our simulations that structural defects can be formed that result in increasing values of ν.

3.4 Microfibril structure prediction

The geometrical features extracted from the atomistic simulations are now used to build a predictive structural model for larger-scale amyloid structures by applying rotation-translation matrices. Figure 8A and 8C shows the resulting fibers for the twofold symmetry morphology obtained imposing the corresponding geometrical parameters listed in Table 1 and extending the rotation and translation of the coordinates over ≈50 nm and ≈500 nm,

respectively. The corresponding fibers are shown in Figure 8B and 8D for the threefold symmetry morphology.

4. Conclusion

Biology utilizes hierarchical structures in an intriguing way to create multifunctional materials. This explains the formation of hierarchical structures with defined length-scales, as can be seen for amyloid protein materials. A hierarchical materials science approach, referred to has materiomics, is a powerful strategy to investigate biological systems from this perspective. We have demonstrated such an approach here in the analysis of the structural properties of amyloid fibrils and fibers at different scales.

Our results provide a direct link between the atomistic details of small fibers to the overall geometric properties of larger ones, facilitating atomistic level structure predictions for mesoscale/microsale amyloid fiber geometries. Specifically, the approach used here provides a novel way forward to link amino acid sequence to structural properties, with measurable geometric effects. It also suggests the importance of the fibril geometry to determine the dominating chemical interactions driving the final configuration and structural properties of the overall fiber. Therefore, the proposed approach could suggest new experimental approaches to try to understand fundamental issues related to the geometry of amyloid growth and structure. Moreover, it provides geometries of amyloid fiber structures at the mesoscale level, which could be studied using other computational techniques (s.a. coarse grained simulations) that allow the analysis of systems with much larger size. Such studies would be critical to examine the mechanical properties of such fibers and utilize them as new novel materials.

Overall, by utilizing self-assembly processes from nano to macro [34], hierarchical structures may be the key that can enable us to take advantage of properties at all scales, and to exploit superior nanoscale properties. Such work has the potential to extend the current state of the art towards developing a new generation of intelligent biomaterials that integrates structure and function, from the nano to macro scales.

Acknowledgements: This research was supported by the Office of Naval Research (grant number NN00014-08-1-0844). We thank Robert Tycko for providing us with atomistic coordinates of twofold and threefold morphology amyloid fibrils.

References

1. Chiti, F. and C.M. Dobson, *Protein misfolding, functional amyloid, and human disease.* Annu. Rev. Biochem., 2006. **75**: p. 333-366.
2. Seilheimer, B., B. Bohrmann, L. Bondolfi, F.Müller, D. Stüber, and H. Döbeli, *The Toxicity of the Alzheimer's Beta-Amyloid Peptide Correlates with a Distinct Fiber Morphology* Journal of Structural Biology, 1997. **119**(1): p. 59-71.
3. Mostaert, A.S., M.J. Higgins, T. Fukuma, F. Rindi, and S.P. Jarvis, *Nanoscale mechanical characterisation of amyloid fibrils discovered in a natural adhesive.* Journal Of Biological Physics, 2006. **32**(5): p. 393-401.
4. Chiti, F., P. Webster, N. Taddei, A. Clark, M. Stefani, G. Ramponi, and C.M. Dobson, *Designing conditions for in vitro formation of amyloid proptofilaments and fibrils.* Proc Natl Acad Sci U S A, 1999. **96**: p. 3590-3594.
5. Fandrich, M. and C.M. Dobson, *The behavior of polyamino acids reveals an inverse side chain effect in amyloid structure formation.* EMBO J., 2002. **21**: p. 5682-5690.
6. Scheibel, T., R. Parthasarathy, G. Sawicki, X.M. Lin, H. Jaeger, and S.L. Lindquist, *Conducting nanowires built by controlled self-assembly of amyloid fibers and selective metal deposition.* Proceedings of the National Academy of Sciences of the United States of America, 2003. **100**(8): p. 4527-4532.
7. Petkova, A.T., Y. Ishii, J.J. Balbach, O.N. Anzutkin, R.D. Leapman, F. Delaglio, and R. Tycko, *A structural model for Alzheimer`s beta-amyloid fibril based on experimental constraints from solid state NMR* PNAS, 2002. **99**(26): p. 16742-16747.
8. Jaroniec, C.P., C.E. MacPhee, N.S. Astrof, C.M. Dobson, and R.G. Griffin, *Molecular conformation of a peptide fragment of transthyretin in an amyloid fibril.* PNAS, 2004. **99**: p. 16748-16753.
9. Paravastu, A., R.D. Leapman, W.-M. Yau, and R. Tycko, *Molecular structural basis for polymorphism in Alzheimer`s Beta-amyloid fibrils.* PNAS, 2008. **105**(47): p. 18349-18354.
10. R. Nelson and M.R. Sawaya and M. Balbirnie and A.O. Madsen and C. Riekel and R. Grothe and D. Eisenberg, *Structure of the cross-beta spine of amyloid-like fibrils.* Nature, 2005. **435**: p. 773-778.
11. Ma, B. and R. Nussinov, *Simulations as analytical tools to understand protein aggregation and predict amyloid conformation.* Current Opinion in Chemical Biology, 2006. **10**: p. 445-452.
12. Nguyen, H.D. and C.K. Hall, *Spontaneous fibril formation by polyalanines; discontinuous molecular dynamics simulations.* J Am Chem Soc 2006. **128**: p. 1890-1901.
13. Buchete, N.V., R. Tycko, and G. Hummer, *Molecular dynamics simulations of Alzheimer's beta-amyloid protofilaments.* J Mol Biol, 2005. **353**: p. 804-821.
14. Han, W. and Y.D. Wu, *A strand-loop-strand structure is a possible intermediate in fibril elongation: long time simulations of amyloid-beta peptide (10-35).* J Am Chem Soc, 2005. **126**: p. 15408-15416.

15. Haspel, N., D. Zanuy, B. Ma, H. Wolfson, and R. Nussinov, *A comparative study of amyloid fibril formation by residues 15-19 of the human calcitonin hormone: a single beta-sheet model with a small hydrophobic core.* J Mol Biol 2005. **345**: p. 1213-1227.
16. Deng, N.J., L. Yan, D. Singh, and P. Cieplak, *Molecular basis for the Cu2+ binding-induced destabilization of {beta}2-microglobulin revealed by molecular dynamics simulation.* Biophys J 2006. **90**: p. 3865-3879.
17. Park, S. and J.G. Saven, *Simulation of pH-dependent edge strand rearrangement in human beta-2 microglobulin.* Protein Science., 2006. **15**.
18. Armen, R.S. and V. Daggett, *Characterization of two distinct beta2-microglobulin unfolding intermediates that may lead to amyloid fibrils of different morphology.* Biochemistry, 2005. **44**: p. 16098-16107.
19. Santini, S. and P. Derreumaux, *Helix H1 of the prion protein is rather stable against environmental perturbations: molecular dynamics of mutation and deletion variants of PrP(90-231).* Cell Mol Life Sci 2004. **61**: p. 951-960.
20. Ma, B. and R. Nussinov, *Stabilities and conformations of Alzheimer's beta -amyloid peptide oligomers (Abeta 16-22, Abeta 16-35, and Abeta 10-35): Sequence effects. .* Proc Natl Acad Sci USA, 2002. **99**: p. 14126-14131.
21. Tycko, R., *Insights into the Amyloid Folding Problem from Solid-State NMR.* Biochemistry, 2003. **42**(11): p. 3151-3159.
22. Paparcone, R. and M.J. Buehler, *Microscale structural model of Alzheimer Abeta(1–40) amyloid fibril.* Appl. Phys. Lett., 2009. **94**: p. 243904.
23. Lazaridis, T. and M. Karplus, *Effective energy function for proteins in solution.* Proteins-Structure Function And Genetics, 1999. **35**(2): p. 133-152.
24. Brooks, B.R., R.E. Bruccoleri, B.D. Olafson, D.J. States, S. Swaminathan, and M. Karplus., *CHARMM: a program for macromolecular energy, minimization, and dynamics calculations.* J. Comp. Chem., 1983. **4**(2): p. 187-217.
25. Periole, X., A. Rampioni, M. Vendruscolo, and A.E. Mark, *Factors that affect the degree of twist in beta -sheet structures: a molecular dynamics simulation study of a cross- beta filament of the GNNQQNY peptide.* J. Phys. Chem. B 2009. **113**: p. 1728–1737.
26. Chothia, C., *"Conformation of twisted Beta-pleated sheets in proteins.* J. Mol. Biol. , 1973. **75**: p. 295-302.
27. Salemme, F.R., *Structural properties of protein beta-sheets.* Prog. Biophys. Mol. Biol. , 1983. **42**: p. 95–133.
28. Maccallum, P.H., R. Poet, and E.J. Milnerwhite, *Coulombic attractions between partially chargedmain-chain atoms stabilise the right-handed twist found in most beta-strands.* J. Mol. Biol., 1995. **248**: p. 374-384.
29. Maccallum, P.H., R. Poet, and E.J. Milnerwhite, J. Mol. Biol., 1995,. **248**: p. 374-384.
30. Chou, K.C., G. Nemethy, and H.A. Scheraga, *Role of interchain interactions in stabilization of the right-handed twist of beta-sheets.* J. Mol. Biol., 1983a. **168**: p. 389-407.
31. Yang, A.S. and B. Honig, *Free Energy Determinants of Secondary Structure Formation: I. a-helices.* J. Mol. Biol. , 1995. **252**: p. 366-376.
32. Wang, L., T. Oconnell, A. Tropsha, and J. Hermans, *Molecular simulations of beta-sheet twisting.* J. Mol. Biol., 1996. **262**: p. 283-293.
33. Koh, E. and T. Kim, *Minimal surface as a model of beta-sheets.* Proteins 2005. **61**: p. 559–569.
34. Reches, M. and E. Gazit, *Peptide Nanomaterials: Self-Assembling Peptides as Building Blocks for Novel Materials*, in *Nanomaterials Chemistry: Novel aspects and*

New Directions, C.N.R. Rao, A. Mueller, and A.K. Cheetham, Editors. 2007, Wiley-VCH: Weinheim. p. 171-183.

Table and Table Caption

Morphology	**Interlayer spacing**, d (in Å)	**Interlayer twist angle,** θ (in degrees)	**Periodicity** ν (in nm)
Twofold	4.79	1.31	131.6
Threefold	4.85	2.12	82.3

Table 1: Extrapolated geometrical values for the interlayer twist angle (θ), interlayer spacing (d) and the periodicity (ν) for the twofold and threefold amyloid fibril morphologies. These parameters can be used to build amyloid fibers of any length (as shown in Figure 8).

Figures and Figure Legends

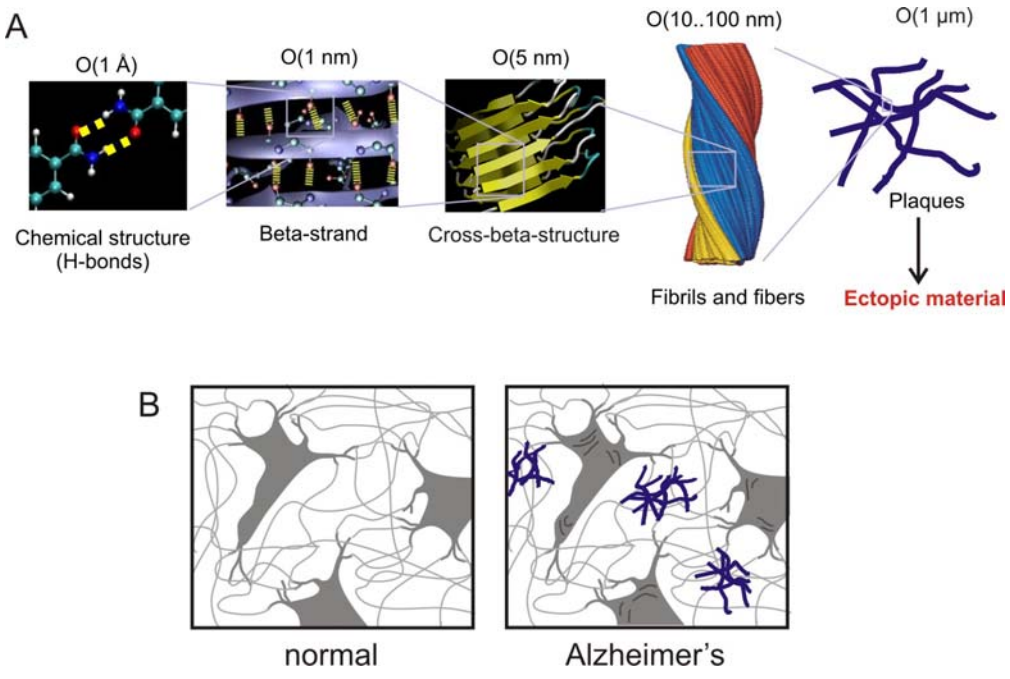

Figure 1: Hierarchical structure of amyloids and structural role in Alzheimer's disease. Panel A shows the hierarchical structure of amyloid plaques, from nano to macro. Panel B shows how amyloid plaques are deposited between neuron cells, influencing the function of brain tissue.

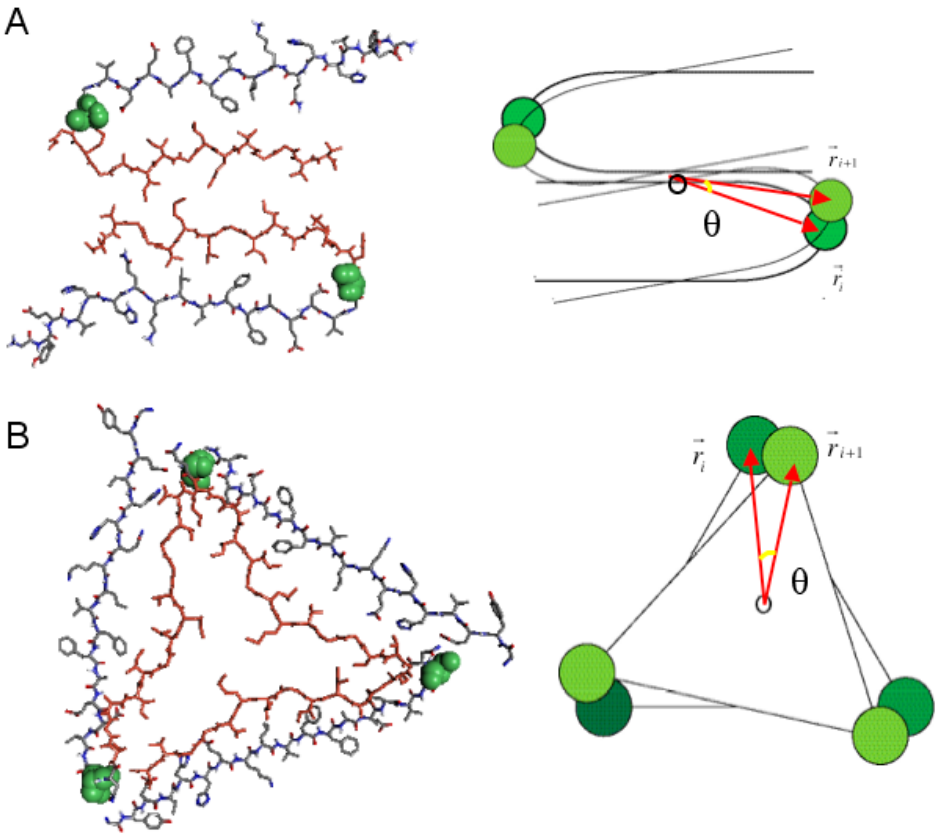

Figure 2: Representation of one layer of the twofold and threefold structures with the corresponding scheme used to calculate the top bottom distance and the twist angle (panels A and B, respectively). The positions of the residues used as reference are represented in green color and in bigger dimensions, while the most hydrophobic part of the amino acid sequence is distinguished by the red color. In all cases the most hydrophobic parts are located towards the interior region of the amyloid fibril.

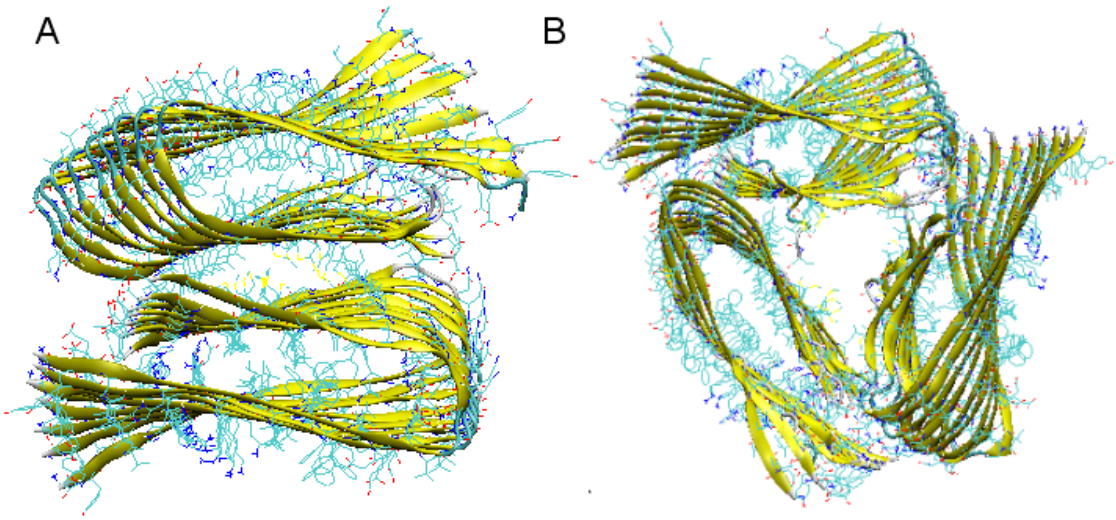

Figure 3: Relaxed amyloid structures with $N = 9$ for the twofold (panel A) and the threefold (panel B) morphology. The two configurations show an evident twist angle around the fiber growth axis.

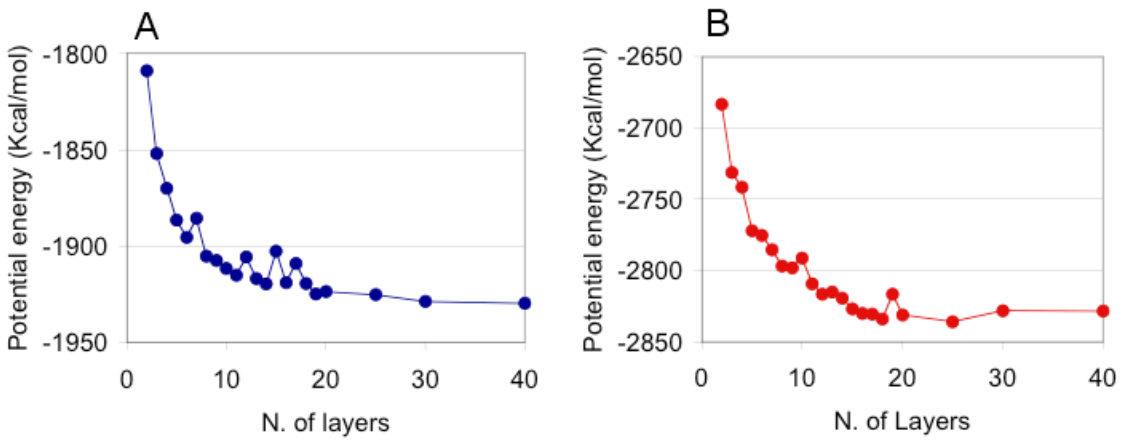

Figure 4: Dependence of potential energy on the fiber length, for the twofold (panel A) and the threefold (panel B) morphologies. Energy values are normalized by the number of layers in both cases.

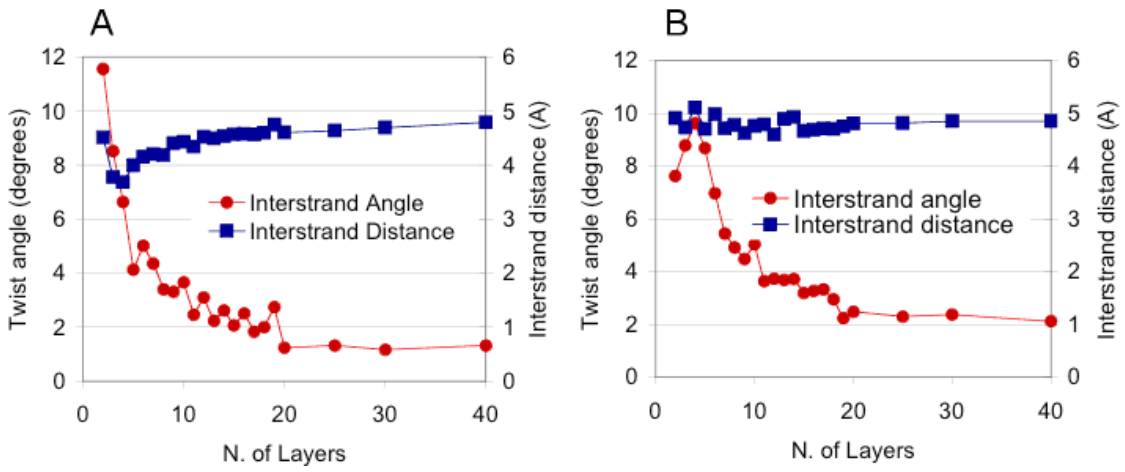

Figure 5: Interstrand distance and twist angle as the fiber length increases for the twofold morphology (panel A) and the threefold one (panel B). All values are normalized by the number of the layers.

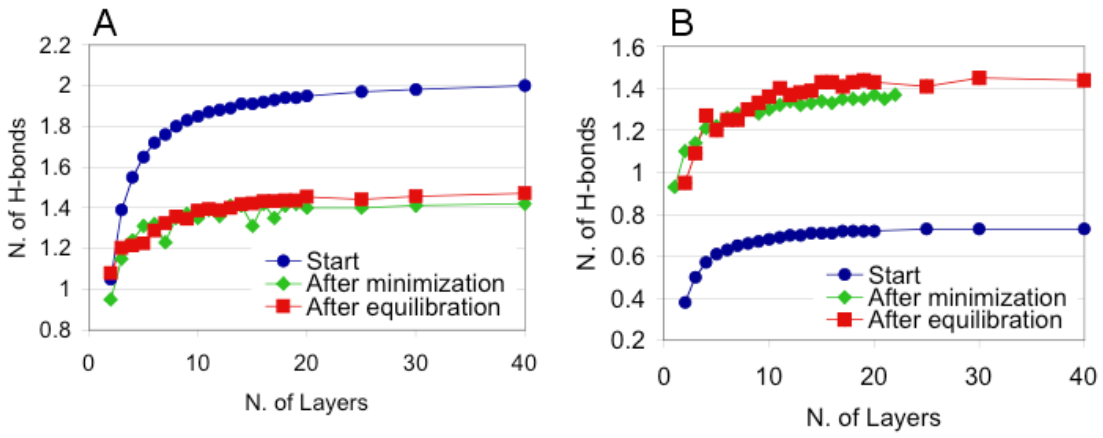

Figure 6: Variation of the number of H-bonds during minimization and relaxation, as a function of the number of layers composing the amyloid fibril. Panels A and B refer to the twofold and three symmetry, respectively. All values are normalized by the number of amino acids. In the twofold morphology (panel A), the number of H-bond decreases with the minimization and the subsequent finite temperature relaxation. The opposite occurs in the threefold structure, suggesting the importance of the intrinsic symmetry and geometry of the fibril.

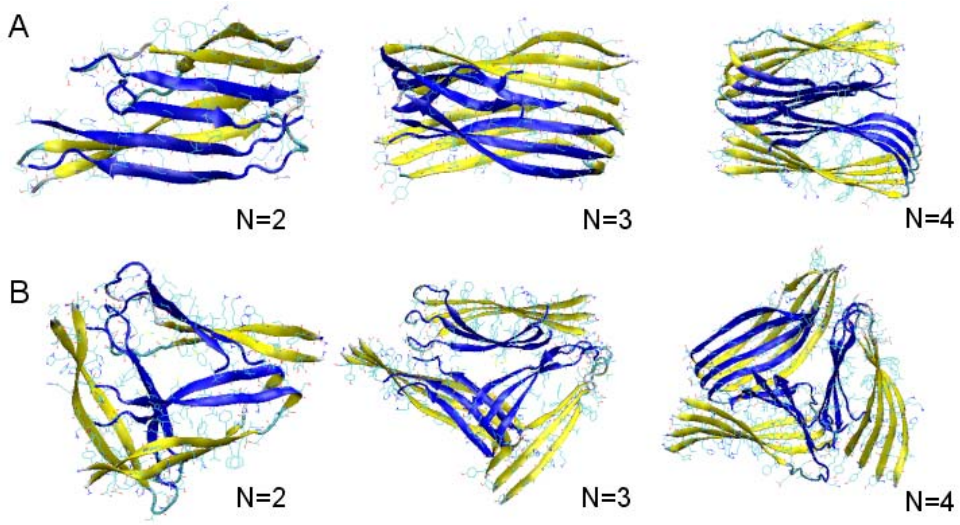

Figure 7: Relaxed structures consisting of 2, 3 and 4 layers for the twofold (A) and the threefold morphology (B). The cartoon visualization method allows one to distinguish the presence of β-sheets even in these short structures. The blue color is used here to indicate the inner part of the chains and to illustrate how the hydrophobic interactions in combination with the H-bonds forming drive the final configurations.

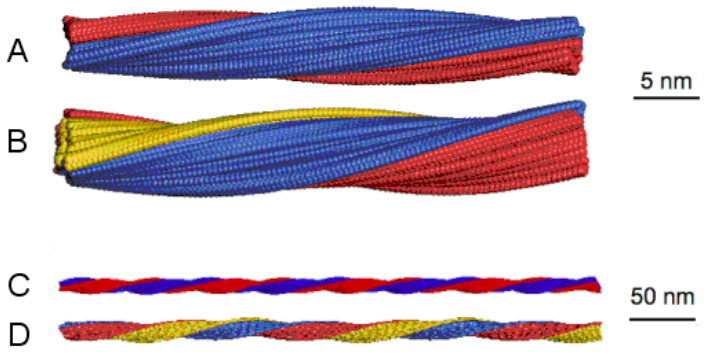

Figure 8: Microscale structure prediction of the twofold and threefold morphology amyloid fibers of ≈50 nm (subplot A and B) and ≈500 nm (subplot C and D) length. The structure reported in subplots A, B, C and D have been obtained using the extrapolated geometrical parameters reported in Table 1 and by applying the rotation-translation matrices to the coordinates of one layer of the same fiber. Different colors are used to distinguish the individual chains from one another. A scale bar for the ≈50 nm fibers (subplots A and B) and for the ≈500 nm fibers (subplots C and D) is included.